

Article

Not peer-reviewed version

Evaluation of Radiation Response in CoCrFeNiNb0.65 Eutectic High-Entropy Alloys

[Yang Wang](#) , [Hongwu Zhu](#) ^{*} , [Yansen Li](#) ^{*} , Anwei Wang

Posted Date: 28 July 2023

doi: 10.20944/preprints2023071999.v1

Keywords: Eutectic high-entropy alloys; ion irradiation; helium bubbles; mechanical properties; nanoindentation



Preprints.org is a free multidiscipline platform providing preprint service that is dedicated to making early versions of research outputs permanently available and citable. Preprints posted at Preprints.org appear in Web of Science, Crossref, Google Scholar, Scilit, Europe PMC.

Copyright: This is an open access article distributed under the Creative Commons Attribution License which permits unrestricted use, distribution, and reproduction in any medium, provided the original work is properly cited.

Article

Evaluation of Radiation Response in $\text{CoCrFeNiNb}_{0.65}$ Eutectic High-Entropy Alloys

Yang Wang ¹, Hongwu Zhu ^{1,*}, Yansen Li ^{2,3,4,*} and Anwei Wang ⁵

¹ College of Mechanical and Transportation Engineering, China University of Petroleum-Beijing, Beijing 102249, China

² Department of Engineering Mechanics, Shijiazhuang Tiedao University, Shijiazhuang 050043, China

³ Hebei Research Center of the Basic Discipline Engineering Mechanics, Shijiazhuang Tiedao University, Shijiazhuang 050043, China

⁴ Hebei Key Laboratory of Mechanics of Intelligent Materials and Structures, Shijiazhuang Tiedao University, Shijiazhuang 050043, China

⁵ School of Astronautics, Harbin Institute of Technology, Harbin 150001, China

* Correspondence: zhuhwcup@163.com (H.Z.); liyansen@stdu.edu.cn (Y.L.)

Abstract: A $\text{CoCrFeNiNb}_{0.65}$ eutectic high-entropy alloys (EHEAs) prepared by arc melting were irradiated with a 100 keV He^+ ion beam. Swelling, helium bubbles and mechanical response induced by irradiation were evaluated. When the ion fluence reached 1.0×10^{18} ions/cm², the irradiation-induced swelling occurred on the sample surface, and as the ion fluence increasing, the swelling became increasingly severe and the surface of Nb-rich phase appeared peeling and shedding. Meanwhile, along the boundaries of matrix and Nb-rich phase there was a neat line of helium bubbles. The size of these helium bubbles decreased with distance from the center of the helium bubble layer. This result indicated that the phase boundaries were favorable sites for the nucleation and gathering of helium bubbles. Nanoindentation results indicated that hardening and softening induced by He^+ ion irradiation occurred in various ion fluences. At ion fluence of 5.0×10^{17} ions/cm², the $\text{CoCrFeNiNb}_{0.65}$ EHEAs shows obvious hardening behavior, which can be explained by dislocation-dominated hardening effect. When the ion fluence reached 1.0×10^{18} ions/cm² and 2.0×10^{18} ions/cm², the hardening effect may be weakened due to the helium bubble aggregation and growth, as well as helium bubbles induced noncompact structures. The results of this study provide insights into the effect of helium bubbles on mechanical evolution and pave the way for designing EHEAs suitable for the nuclear industry.

Keywords: eutectic high-entropy alloys; ion irradiation; helium bubbles; mechanical properties; nanoindentation

1. Introduction

High entropy alloy (HEA) is a new type of alloy, which has attracted great attention in the past decades because of its excellent physical and chemical properties, and is considered as a new type of structural material[1-3]. Extensive research has evaluated the radiation resistance of HEAs, focusing on the comparison of phase stability and dimensional stability between HEAs and traditional alloys[4-6]. For example, CoCrFeNiMn HEA with a single FCC phase shows enhanced radiation resistance by inhibiting void formation, and has 40 times higher expansion resistance than nickel at high temperature[7]. Under the irradiation of 723 K, the He bubble size (4.0 nm) formed in CoCrFeNiMn is obviously smaller than that in 304 stainless steel (5.5 nm)[8]. With the increase of Al content, the structure of $\text{Al}_x\text{CoCrFeNi}$ HEAs changes from FCC to FCC+BCC, and then to BCC. Compared with conventional nuclear materials, $\text{Al}_x\text{CoCrFeNi}$ HEAs shows excellent structural stability and volume expansion resistance[9]. Meanwhile, researchers in HEAs turn to develop multiphase HEAs to improve its radiation tolerance and mechanical properties, but this usually leads to poor castability[10].

In recent years, eutectic high-entropy alloys (EHEAs) have been studied more and more widely. In addition to being a novel method for obtaining composite structures in HEAs, eutectic alloys are

also considered good candidates for superalloys because the eutectic solidification microstructure has the following characteristics: 1) the microstructure is close to equilibrium, that is, it can resist changes at the same high temperature as its reaction temperature; 2) low-energy phase boundaries; 3) controllable microstructures; 4) high fracture strength; 5) the defect structure is stable; 6) good high temperature creep resistance[11]. In addition, eutectic alloy also has good castability. the AlCoCrFeNi_{2.1} EHEA has attracted much attention because of its good strength, ductility and excellent thermodynamic properties[11]. The atomic scale irradiation response of AlCoCrFeNi_{2.1}, which consists of face-centered cubic (FCC) phase and B2 phase, has been systematically studied by Pang et al[12]. The results show that, compared with B2 structure, disordered FCC phase has stronger ability to inhibit the nucleation and growth of He bubbles. Another eutectic component that has received more attention is CoCrFeNiNb_x EHEA. He et al.[13] reported that CoCrFeNiNb_x EHEAs with attenuated layered structure maintained good strength and ductility, and the layered structure was stable below 750 °C, but rapidly coarsened at 900 °C. The deformation mechanism of CoCrFeNiNb_x during high pressure torsional deformation was studied by nanoindentation experiment.[14] It was suggested that the high pressure torsion process could obtain EHEAs of ultra-high strength while preserving the excellent plasticity of the alloy at room temperature.

At present, there are few studies on the evolution of mechanical properties of EHEAs after irradiation. Meanwhile, most studies focus on the influence of composition on radiation-induced expansion and radiation damage, while the micro-changes of EHEAs induced by radiation, such as the evolution of helium bubbles, are rarely reported. In this study, the typical CoCrFeNiNb_{0.65} EHEA is selected, the main purpose is to determine the irradiation response of He⁺ ion irradiation, and some interesting phenomena are explained. In this study, the basic irradiation behavior of EHEA materials was studied, and the potential of this series of materials in extreme environment was deeply understood.

2. Materials and Methods

CoCrFeNiNb_{0.65} EHEAs prepared via arc melting 99.99% pure elemental constituents together in a high purity argon atmosphere. The ingots were inverted and melted repeatedly to ensure homogeneity and subsequently suck-casted into a water-cooled copper mold (45 mm). Then Φ5 mm cylindrical rods were cut into wafer samples with 2.0 mm thickness, and then mechanically polished to a mirror finish. Irradiation experiments were conducted in the 320 kV multidiscipline research platform for highly-charged ions (Institute of Modern Physics, Chinese Academy of Sciences, Lanzhou, China), at a pressure near or below 10⁻⁵ torr. The polished samples were irradiated with a 100 keV He⁺ ion beam, with ion fluences of 5.0×10¹⁷ ions/cm², 1.0×10¹⁸ ions/cm², and 2.0×10¹⁸ ions/cm², respectively, at room temperature.

Figure 1 shows the results of ion distribution, radiation damage (displacement per atom or dpa) and He atom concentration increasing with depth calculated using the Ion Distribution and Quick Calculation of Damage mode in the SRIM (Stopping and Range of Ions in Matter) 2008 code[15]. As shown in Figure 1, when a large number of incident ions enter EHEAs, they form a spatial influence area instead of a specific path due to collision cascade. The total number of ions is 99,999, and the effective depth of ion influence is ~500 nm. The dpa is determined by the predicted vacancy concentrations of Co, Cr, Fe, Ni and Nb and the sum of recoil events in the range of ~500 nm from the surface. In addition, the number of atomic shifts reaches a peak at a depth of about 290 nm, which corresponds to the projection range of He⁺ ions in CoCrFeNiNb_{0.65} EHEAs. Under the influence of 5.0×10¹⁷ ions /cm², the peak concentration of He atoms is about 22.0%.

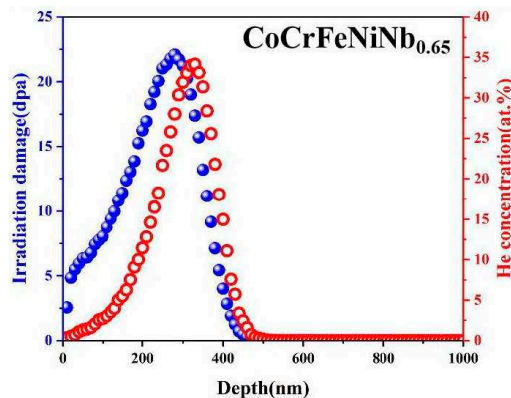


Figure 1. Damage of CoCrFeNiNb_{0.65} EHEAs irradiated by He irradiation at 5.0×10^{17} ions/cm².

The microstructures were characterized by X-ray diffraction (XRD) via a Philips PW 1050 diffractometer with Cu-K α radiation operating at 45 keV, a 0.01 step size, and a 200 mA current for phase analysis with improved accuracy. The diffraction area of sample surface is 0.5 mm, and the scanning speed is 2°/min. Each sample was examined three times in different areas.

The microstructure and composition of the samples were analyzed by a scanning electron microscopy (SEM, HITACHI S-4800, Tokyo, Japan) at a working voltage of 20.0 kV and a working distance of 15.8 mm, with energy-dispersive X-ray spectroscopy (EDX, HORIBA X-Max, Kyoto, Japan). Transmission electron microscopy (TEM) observations were performed via an FEI Tecnai G2 microscope operating at 200 kV to investigate the microstructural evolution of the samples. The cross-sectional TEM samples were obtained via the gallium focused-ion beam (FIB, Helios Nanolab 600) lift-out technique on a ZEISS Auriga FIB-SEM workstation.

To investigate the ion irradiation-induced microstructural evolution of EHEAs, nanoindentation experiments were conducted on pristine and irradiated samples using an Agilent Technologies Nano Indenter G200 with a Berkovich diamond indenter at 20°C after calibration on standard fused silicon. The loading rate was 0.05 mN/s, with a maximum loading of 20 mN.

3. Results

3.1. Microstructural Characterization

The XRD patterns of the pristine and irradiated CoCrFeNiNb_{0.65} EHEA samples at different fluences are presented in Figure 2. The results indicated that the alloys are composed of FCC and Laves phases. And no obvious phase decomposition occurred under any irradiation condition, which is consistent with high configurational entropy playing a significant role in phase stability.

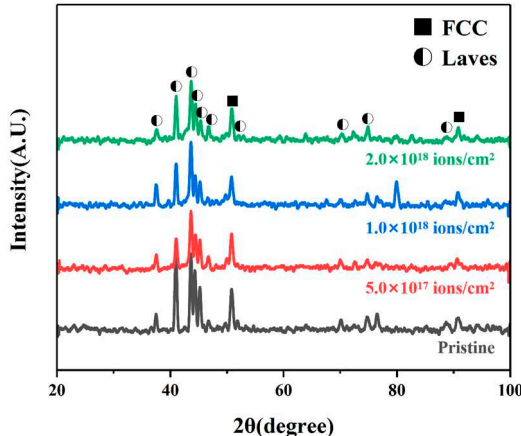


Figure 2. XRD patterns for pristine and irradiated samples at various fluences.

3.2. Surface Topography

The SEM images reveal the surface morphology of pristine and irradiated CoCrFeNiNb_{0.65} EHEAs at various fluences, as shown in Figure 3a-d. According to the SEM results indicate the surface morphology of the samples is mainly composed of two phases, matrix phase and petal-like Nb-rich phase. The surface of the sample did not change significantly at the fluence of 5.0×10^{17} ions/cm². As the ion fluence reaching 1.0×10^{18} ions/cm², it is easy to find some obvious bubbles in the matrix phase region, which is due to the surface bubbling induced by He ion irradiation. However, when the ion fluence was as high as 2.0×10^{18} ions/cm², the number of bubbles increased significantly. It should be noted that at this fluence, the Nb-rich phase also began to show large shedding, exposing the lower surface after peeling. This peeling phenomenon after irradiation is mainly due to the low energy and high fluence of He ions injected into the material, which have a relatively shallow incidence range due to the low incidence energy of ions, and the accumulated helium bubbles induced by high fluence He injection will gradually move to the surface, eventually leading to swelling and peeling of the surface, which also suggested that the degree of swelling varied between the two phases under the same irradiation condition.

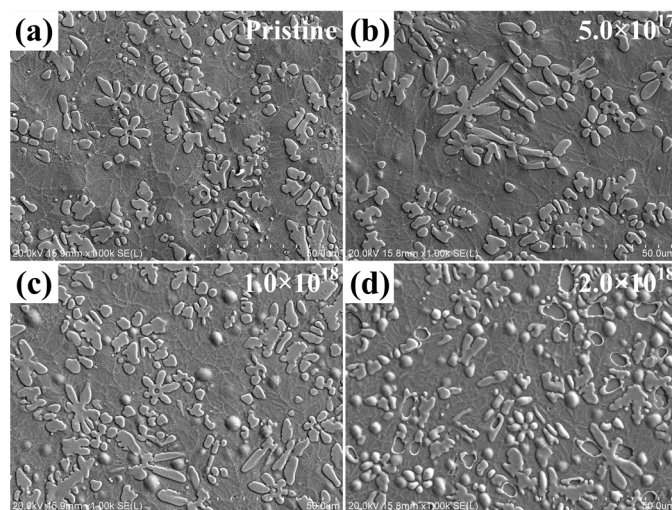


Figure 3. The SEM images of CoCrFeNiNb_{0.65} at fluences of (a) 0, (b) 5.0×10^{17} ions/cm², (c) 1.0×10^{18} ions/cm² and (d) 2.0×10^{18} ions/cm².

The microstructure of the irradiated EHEAs was further studied by TEM. Figure 4a shows the TEM bright-field profiles of irradiated samples prepared by FIB at the fluence of 1.0×10^{18} ions/cm². Figure 4b shows the TEM bright-field images of the irradiated regions at high magnifications. And the corresponding elemental distribution of Co, Cr, Fe, Ni and Nb are shown in Figure 4c. The light and dark stripes in the photo correspond to the matrix phase and the Nb-rich phase in the material, respectively. In particular, a clear layer of helium bubbles appears about 500 nm from the surface of the sample, as shown by the yellow line in Figure 4a, and the size of the helium bubble increases from the sides of the helium bubble layer to the center. Surprisingly, along the boundaries of matrix and Nb-rich phase there is a neat line of helium bubbles that is longer than the width of the helium bubble. The closer the helium bubble is to the center, the larger the size of the helium bubble is. And the farther away the bubble is from the center, the smaller it gets, until it disappears. This kind of helium bubble aggregation behavior is common in the irradiation study of nanometer multilayer composites. Previous work has shown that helium bubbles and cavities preferentially form in the grain boundaries of ultrafine and nanocrystalline tungsten, as well as other composite structures[16-20]. Li et al.[21] found that helium bubbles gathered along the Fe/W interface by irradiating Fe/W nanolayered composites with He ions. In fact, defects such as dislocations, voids and interfaces act as nucleation sites for irradiation-induced point defects in the early stages of helium bubble formation. Dislocations absorb more gaps than vacancies, and thus are preferred regions for helium bubble nucleation. Singh et al.[22] suggested that the effect of grain size on radiation damage was mainly

due to the depletion of vacancies within grains and their migration to grain boundaries. And vacancy clusters grow and capture He to form helium bubbles. Similar to grain boundaries, the phase boundary in this study also appears to be a favorable location for helium bubble nucleation. Therefore, helium bubbles accumulate along the phase boundary and form a small to large arrangement with the trend of He concentration.

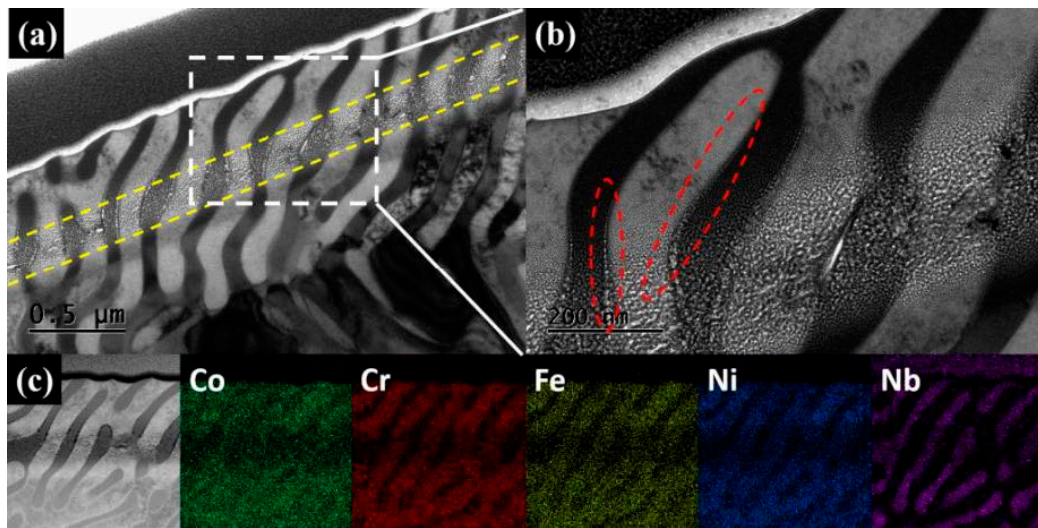


Figure 4. (a) TEM images of CoCrFeNiNb_{0.65} EHEAs at 1.0×10¹⁸ ions/cm²; (b) the magnification picture in the white dotted box; (c) EDX mapping results.

3.3. Mechanical behavior

The average microhardness of CoCrFeNiNb_{0.65} EHEAs surface was measured by nano-indentation method and the radiation hardening behavior was studied. Figure 5 shows typical depth profiles of nanoindentation hardness of pristine and irradiated CoCrFeNiNb_{0.65} EHEAs at different irradiation fluence. The matrix phase and the Nb-rich phase of the sample were selected for hardness measurement respectively. As shown in Figure 5, irradiation-induced hardening occurred in both matrix phase and the Nb-rich phase at the fluence of 5.0×10¹⁷ ions/cm². With the ion fluence increasing to 1.0×10¹⁸ ions/cm² and 2.0×10¹⁸ ions/cm², as the radiation fluence continued to increase, the irradiation induced hardening behavior gradually weakened, and softening appeared.

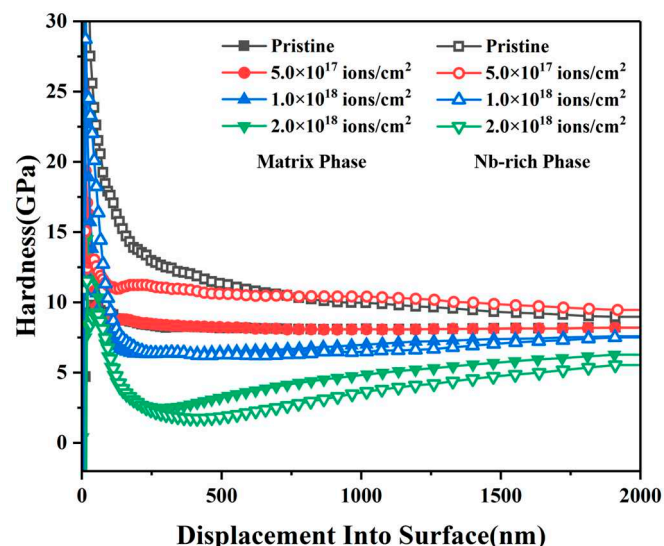


Figure 5. Typical depth profiles of nanoindentation hardness of pristine and He⁺ ion-irradiated CoCrFeNiNb_{0.65} EHEAs at various irradiation fluences.

4. Discussion

The schematic in Figure 6 illustrates the radiation response of CoCrFeNiNb_{0.65} EHEAs during He⁺ irradiation. Normal dislocation slip occurred within the pristine sample when indented into the sample surface, as shown in Figure 6a. According to Figure 6b, at the fluence of 5.0×10¹⁷ ions/cm², CoCrFeNiNb_{0.65} EHEAs exhibit marked hardening behavior. Generally, in crystalline materials, irradiation-induced hardening is attributed to the interaction between irradiation-induced defects, and two types of approximate defect obstruction models have been used: the Orowan model[23,24] for strong barriers (i.e., interstitials, interstitial loops, and precipitates); Friedel-Kroupa-Hirsch (FKH) model[21,25] for weak barriers (i.e., helium bubbles). According to dislocation theory, the critical pressure for exiting a dislocation loop from the surface of a helium bubble can be expressed as,

$$P_c = \frac{2\gamma}{r} + \frac{\mu b}{r}, \quad (1)$$

Where, γ is the surface free energy. Once the internal pressure of the helium bubble is greater than the critical pressure, it sprints out of the dislocation loops, which impede the movement of the dislocation:

$$\tau_{DL} = \mu b \sqrt{h_p \rho_p d_p}, \quad (2)$$

Where, h_p is the coefficient of dislocation ring hardening. ρ_p and d_p are the density and size of the dislocation ring, respectively, depending on the size, internal pressure and density of the corresponding helium bubble. For the FKH model in crystalline materials, it can be written as,

$$\Delta\sigma = \frac{1}{8} M \mu b d N^{2/3} \quad (3)$$

Where, M is the Taylor factor, μ is the shear modulus, and b is the Burgers vector. Therefore, the formation and evolution of helium bubbles at the initial stage of irradiation have made some contributions to irradiation-induced hardening. On the other hand, although some He atoms have been combined with vacancy to form He bubbles in CoCrFeNiNb_{0.65} EHEAs, there are still a large number of isolated He atoms or He clusters in the system. Research[26] shows that at low temperature, interstitial atoms near dislocations can easily migrate to the dislocation core, thus preventing dislocation from slipping. In addition, according to early studies of helium bubbles[27-29], the elastic interaction between two pressurized bubbles causes an attractive force between them. With the rapid growth of helium bubbles, the attraction between them increases, which increases the internal stress within the matrix and may lead to an increase in hardening in the He concentration region. Given the difficulty in estimating the small radiation hardening of helium bubbles and measuring the density of dislocation loops, the explanation of the radiation-induced hardening mechanism in CoCrFeNiNb_{0.65} EHEA is complicated. However, radiation-induced hardening may result primarily from dislocation loops and interstitial atoms, as well as the interaction between helium bubbles and dislocations.

In this study, it is suggested that as the helium bubble grows and exceeds the critical size with the fluence increased up to 1.0×10¹⁸ ions/cm² and 2.0×10¹⁸ ions/cm², the region near the helium bubble does not provide enough space for its continuous growth, and the overlapping helium bubble may negatively affect the local hardening of CoCrFeNiNb_{0.65} EHEA, as shown in Figure 6c. Furthermore, the continuous coalescence and overlap of helium bubbles may cause large voids or open volume regions in the helium bubble layer, eventually leading to softening due to structural collapse. Meanwhile, this process is also accompanied by swelling and peeling of the sample surface, which is consistent with the microscopic morphology in Figure 3.

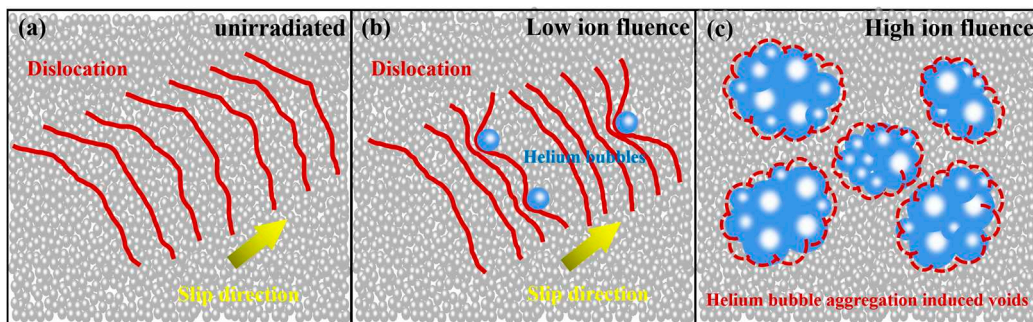


Figure 6. Typical depth profiles of nanoindentation hardness of pristine and He^+ ion-irradiated $\text{CoCrFeNiNb}_{0.65}$ EHEAs at various irradiation fluences.

5. Conclusions

$\text{CoCrFeNiNb}_{0.65}$ EHEAs prepared by arc melting were irradiated with a 100 keV He^+ ion beam at fluences of 5.0×10^{17} ions/cm², 5.0×10^{17} ions/cm², and 1.0×10^{18} ions/cm² at room temperature. XRD results proved that $\text{CoCrFeNiNb}_{0.65}$ EHEAs are composed of FCC and laves phases. And no obvious phase decomposition occurred under any irradiation condition, which is consistent with high configurational entropy playing a significant role in phase stability. The SEM results indicated the surface morphology of the samples was mainly composed of two phases, matrix phase and petal-like Nb-rich phase. When the ion fluence increased to 1.0×10^{18} ions/cm², the irradiation-induced swelling occurred on the sample surface, and as the fluence increasing to 2.0×10^{18} ions/cm², the swelling became increasingly severe and the surface of Nb-rich phase appeared peeling and shedding, which suggested that the degree of swelling varied between the two phases under the same irradiation condition. TEM results showed an interesting result that along the boundaries of matrix and Nb-rich phase there was a neat line of helium bubbles that was longer than the width of the helium bubble. The closer the helium bubble is to the center, the larger the size of the helium bubble was. And the farther away the bubble was from the center, the smaller it gets, until it disappeared, which was common in the irradiation study of nanometer multilayer composites. Nanoindentation was performed to indicate that hardening and softening induced by He^+ ion irradiation occurred in various ion fluences. At ion fluence of 5.0×10^{17} ions/cm², the $\text{CoCrFeNiNb}_{0.65}$ EHEAs exhibited an obvious hardening behavior, which can be explained by dislocation-dominated hardening effect. When the ion dose reached 1.0×10^{18} ions/cm² and 2.0×10^{18} ions/cm², the hardening effect decreased probably due to the helium bubble aggregation and growth, as well as helium bubbles induced noncompact structures.

Author Contributions: Conceptualization, Y.L. and Y.W.; software, H.Z.; validation, Y.L. and Y.W.; formal Analysis, Y.W.; investigation, Y.W. and Y.L.; resources, A.W.; data curation, Y.W. and H.Z.; writing-original draft preparation, Y.W.; writing-review & editing, Y.W. and Y.L.; visualization, Y.W.; supervision, A.W. and Y.L.; project administration, H.Z. and Y.L.

Funding: This work was supported by the National Natural Science Foundation of China (Grant No. 51401028, No. 51271193, No. 11402277, No. 11790292) and the Strategic Priority Research Program of the Chinese Academy of Sciences (Grant No. XDB22040303). This work was also supported by the Innovation Program (237099000000170004).

Conflicts of Interest: The authors declare no conflict of interest.

References

- Yeh, J.W.; Chen, S.K.; Lin, S.J.; Gan, J.Y.; Chin, T.S.; Shun, T.T.; Tsau, C.H.; Chang, S.Y. Nanostructured High-Entropy Alloys with Multiple Principal Elements: Novel Alloy Design Concepts and Outcomes. *Advanced Engineering Materials* **2004**, *6*, 299-303.
- Cantor, B.; Chang, I.T.H.; Knight, P.; Vincent, A.J.B. Microstructural development in equiatomic multicomponent alloys. *Materials Science and Engineering: A* **2007**, *375-377*, 213-218.
- Zhang, Y.; Zuo, T. T.; Tang, Z.; Gao, M.C.; Dahmen, K.A.; Liaw, P.K.; Lu, Z.P. Microstructures and properties of high-entropy alloys. *Progress in materials science* **2014**, *61*, 1-93.

4. Wang, Y.; Zhang, K.; Feng, Y.H.; Li, Y.S.; Tang, W.Q.; Zhang, Y.T.; Wei, B.C.; Hu, Z. A. Excellent irradiation tolerance and mechanical behaviors in high-entropy metallic glasses. *Journal of Nuclear Materials* **2019**, 527, 151785.
5. Wang, Y.; Zhang, K.; Feng, Y.H.; Li, Y.S.; Tang, W.Q.; Zhang, Y.T.; Wei, B.C.; Hu, Z. Mechanism of local hardening in metallic glass during He ion irradiation. *Materialia* **2020**, 11, 100691.
6. Zhang, Y.; Zhou, Y.J.; Lin, J.P.; Chen, G.L.; Liaw, P.K. Solid-solution phase formation rules for multi-component alloys. *Advanced engineering materials* **2008**, 10, 534-538.
7. Lu, C.Y.; Niu, L.L.; Chen, N.J.; Jin, K.; Yang, T.N.; Xiu, P.Y.; Zhang, Y.W.; Gao, F.; Bei H.B.; Shi, S.; He, M.R.; Robertson, I.M.; William, J.W.; Wang, L.M. Enhancing radiation tolerance by controlling defect mobility and migration pathways in multicomponent single-phase alloys. *Nature Communications* **2016**, 7, 13564.
8. Li, N.; Huang, S.; Zhang, G.D.; Qin, R.Y.; Liu, W.; Xiong, H.P.; Shi, G.Q.; Blackburn, J. Progress in additive manufacturing on new materials: a review. *Journal of Materials Science & Technology* **2015**, 35, 242-269.
9. Zhang, Y.; Yang, T.F.; Xia, S.Q.; Liu, S.X. Irradiation Resistance in $Al_xCoCrFeNi$ High Entropy Alloys. *JOM* **2015**, 67, 2340-2344.
10. Lu, Y.P.; Dong, Y.; Jiang, H.; Wang, Z.J.; Cao, Z.Q.; Guo, S.; Wang, T.M.; Li, T.J.; Liaw, P.K. Promising properties and future trend of eutectic high entropy alloys. *Scripta Materialia* **2020**, 187, 202-209.
11. Lu, Y.P.; Dong, Y.; Guo, S.; Jiang, L.; Kang, H.J.; Wang, T.M.; Wen, B.; Wang, Z.J.; Jie, J.C.; Cao, Z.Q.; Ruan, H.H.; Li, T.J. A Promising New Class of High-Temperature Alloys: Eutectic High-Entropy Alloys. *Scientific Reports* **2014**, 4, 6200.
12. Pang, J.Y.; Xiong, T.; Yang, W.F.; Ge, H.L.; Zheng, X.D.; Song, M.; Zhang, H.W.; Zheng, S.J. Atomic scale structure dominated FCC and B2 responses to He ion irradiation in eutectic high-entropy alloy $AlCoCrFeNi_{21}$. *Journal of Materials Science & Technology* **2022**, 129, 87-95.
13. He, F.; Wang, Z.J.; Shang, X.L.; Leng, C.; Li, J.J.; Wang, J.C. Stability of lamellar structures in $CoCrFeNiNb_x$ eutectic high entropy alloys at elevated temperatures. *Materials & Design* **2016**, 104, 259-264.
14. Maity, T.; Prashanth, K.G.; Balçi, Ö.; Wang, Z.; Jia, Y.D.; Eckert, J.H. Plastic deformation mechanisms in severely strained eutectic high entropy composites explained via strain rate sensitivity and activation volume. *Composites Part B: Engineering* **2018**, 150, 7-13.
15. Egeland, G.W.; Valdez, J.A.; Maloy, S.A.; McClellan, K.J.; Sickafus, K.E.; Bond, G.M. Heavy-ion irradiation defect accumulation in ZrN characterized by TEM, GIXRD, nanoindentation, and helium desorption. *Journal of Nuclear Materials* **2013**, 435, 77-87.
16. Shi, Y.Z.; Jiang, Z.Y.; Xia, T.J.; Zhang, W.J.; Yang, P.S.; Ren, X.Y.; Wang, M.Q.; Liang, L.S.; Cao, X.Z.; Zhu, K.G. Helium diffusion and bubble evolution in single-phase tungsten-based W-Ta-Cr-V complex concentrated alloy. *Journal of Nuclear Materials* **2023**, 578, 154335.
17. Jiang, W.L.; Kovarik, L.; Kruska, K.; Fu, Y.C.; Hu, Z.H.; Shao, L.; Setyawan, W. Behavior and properties of helium cavities in ductile-phase-toughened tungsten irradiated with He^+ ions at an elevated temperature. *Materialia* **2023**, 29, 101789.
18. Pu, G.; Sun, H.X.; Wang, Y.H.; Li, J.; Du, X.J.; Liu, B.; Ren, D.; Zhang, K.; Li, G.Z.; Lin, L.W. Effect of periodic thickness on the helium bubble evolution and irradiation hardening in Cu/W(Re) multi-layered films under helium ion irradiation. *Journal of Alloys and Compounds* **2023**, 935, 167978.
19. Lv, S.S.; Shen, Y.H.; Zhu, R.; Zhou, Q.; Shi, L.; Sun, L.B.; Li, Z.C. The irradiation effects on the nanoindentation hardness and helium bubbles evolution mechanism of Ni-based alloy. *Radiation Physics and Chemistry* **2023**, 206, 110763.
20. Jiang, M.H.; Mir, A.H.; Bahri, M.; Zhang, Y.J.; Browning, N.; Whittle, K.; Patel M. Helium bubbles in $Gd_2Ti_2O_7$ borosilicate glass-ceramic composites. *Journal of Nuclear Materials* **2023**, 581, 154424.
21. Li, N.; Fu, E.G.; Wang, H.; Carter, J.J.; Shao, L.; Maloy, S.A.; Misra, A.; Zhang, X. He ion irradiation damage in Fe/W nanolayer films. *Journal of Nuclear Materials* **2009**, 389, 233-238.
22. Singh, B. N. Effect of grain size on void formation during high-energy electron irradiation of austenitic stainless steel. *Philosophical Magazine* **1974**, 29, 25-42.
23. Yu, L.; Xiao, X.Z.; Chen, L.R.; Chu, H.J.; Duan, H.L. A micromechanical model for nano-metallic-multilayers with helium irradiation. *International Journal of Solids and Structures* **2016**, 102-103, 267-274.
24. Dérès, J.; Proville, L.; Marinica, M.C. Dislocation depinning from nano-sized irradiation defects in a bcc iron model. *Acta Materialia* **2015**, 99, 99-105.
25. Zinkle, S.J.; Matsukawa, Y. Observation and analysis of defect cluster production and interactions with dislocations. *Journal of Nuclear Materials* **2004**, 329-333, 88-96.
26. Orowan, E. Symposium on Internal Stresses in Metals and Alloys; Institute of Metals: London, UK, **1948**.
27. Seeger, A.K. On the theory of radiation damage and radiation hardening. In Proceedings of the Second United Nations International Conference on the Peaceful Uses of Atomic Energy, Geneva, Switzerland, 1-13 September **1958**, 250-273.
28. Grossbeck, M.L.; Maziasz, P.J.; Rowcliffe, A.F. Modeling of strengthening mechanisms in irradiated fusion reactor first wall alloys. *Journal of Nuclear Materials* **1992**, 191-194, 808-812.

29. Garner, F.A.; Hamilton, M.L.; Panayotou, N.F.; Johnson, G.D. The microstructural origins of yield strength changes in aisi 316 during fission or fusion irradiation. *Journal of Nuclear Materials* **1981**, *104*, 803-807.

Disclaimer/Publisher's Note: The statements, opinions and data contained in all publications are solely those of the individual author(s) and contributor(s) and not of MDPI and/or the editor(s). MDPI and/or the editor(s) disclaim responsibility for any injury to people or property resulting from any ideas, methods, instructions or products referred to in the content.